Supporting Information

Ueda et al. 10.1073/pnas.0911482107

SI Materials and Methods

Development of a Software, KbiFlow, for Quantitative Analysis of Endoplasmic Reticulum Streaming. To measure the velocity of endoplasmic reticulum (ER) streaming, an optical flow analysis was performed based on cross-correlation function (1, 2). As a preprocessing stage, immobile components were filtered by the subtraction of temporal-averaged image (3).

$$\mathrm{I}(x,y,t) = \mathrm{I}_{\mathrm{raw}}(x,y,t) - \sum_{t'=0}^{T-1} \frac{\mathrm{I}_{\mathrm{raw}}(x,y,t')}{T}, \qquad [S1]$$

where $\mathrm{I}_{\mathrm{raw}}$ is the original stack, I is the preprocessed stack, T is the total number of frames (100), x and y are spatial variables, and t is a temporal variable (frame index). Next, we measured the velocity vector for each pixel using spatial-temporal correlation analysis. To reduce the error vectors, a 3×3 median filter was applied as a postprocessing stage. As a result, a velocity map, F, was obtained for each stack.

$$\Delta\mathrm{I}(x,y,t) = \mathrm{I}(x,y,t) - \frac{\sum_{u,v\in N} \mathrm{I}(x+u,y+v,t)}{\|N\|}, \qquad [S2]$$

$$\mathrm{Corr}_{\mathrm{average}}(x,y,\tau,\xi,\eta) = \sum_{t=0}^{T-1-\tau} \frac{\sum_{u,v\in N} \Delta\mathrm{I}(x+u,y+v,t)\ \cdot \Delta\mathrm{I}(x+u+\xi,y+v+\eta,t+\tau)}{(T-\tau)\sqrt{\sum_{u,v\in N} \Delta\mathrm{I}(x+u,y+v,t)^2 \cdot \sum_{u,v\in N} \Delta\mathrm{I}(x+u+\xi,y+v+\eta,t+\tau)^2}}, \qquad [S3]$$

$$\vec{F}(x,y) = \underset{u,v\in(-1,0,+1)}{\mathrm{median}} \left[\sum_{\tau=1}^{T-1} \frac{\underset{\vec{f}=(\xi,\eta)\in N}{\mathrm{argmax}} \{\mathrm{Corr}_{\mathrm{average}}(x+u,y+v,\tau,\xi,\eta)\}}{\tau(T-1)} \right], \qquad [S4]$$

where $\Delta\mathrm{I}$ is relative intensity, $\mathrm{Corr}_{\mathrm{average}}$ is the temporal ensemble of the spatiotemporal correlation function, ξ and η are spatial lag variables, τ is the temporal lag variable, f is the velocity vector, F is the map of velocity vectors, N consists of 16 $\times$ 16 neighbor pixels ($-8 < u,v \le +8$) and $\|N\|$ is 256.

The velocity map F contained ER regions and non-ER regions, such as vacuoles and extracellular regions. Because the non-ER regions were not necessary for velocity analysis of ER, we generated a mask image M to remove the non-ER regions.

$$\mathrm{M}(x,y) = \begin{cases} 1 \ \textit{if}\ 1 - 2\mathrm{Corr}_{\mathrm{average}}(x,y,1,0,0) \\ \qquad +\mathrm{Corr}_{\mathrm{average}}(x,y,2,0,0) < n, \\ 0 \ \textit{otherwise} \end{cases} \qquad [S5]$$

where n is the threshold of the noise component ($n = 0.8$ for the statistical analysis of ER streaming in Fig. 1*M* and Table S1 and $n = 0.95$ for the generation of the velocity distribution maps). To calculate an average velocity and a maximal velocity, we applied the mask image M to the velocity map F using the following equations.

$$\mathit{Velocity}_{\mathrm{average}} = \frac{\sum_{x,y\in all} \mathrm{M}(x,y)\ |\vec{F}(x,y)|}{\sum_{x,y\in all} \mathrm{M}(x,y)}, \qquad [S6]$$

$$\mathit{Velocity}_{\max} = \max_{x,y\in all} \{\ \mathrm{M}(x,y)\ |\vec{F}(x,y)|\}. \qquad [S7]$$

ER streaming was analyzed using our in-house developed plug-in package for ImageJ software. Calculation and statistical analysis of velocities were performed by KbiFlow plug-in (Eq. **S1**–**S4**, **S6**, and **S7**). Mask images were generated from the "estimateNoise" mode of KbiStkFilter plug-in (Eq. S5). The KBI plug-in package can be downloaded for free from http://hasezawa.ib.k.u-tokyo.ac.jp/zp/Kbi/ImageJKbiPlugins. Scheme of velocity analysis for ER streaming is shown in Fig. S1.

Quantitative Analysis of Cytosol Streaming. Cytosol streaming was analyzed by the KbiFlow plug-in essentially as the analysis of ER streaming. Because of low signal-to-noise ratio in this analysis, we increased the threshold of the noise component to 0.9 and selected the cells having more than 100 successful measurement points.

Image Analysis of Actin Filament Bundles. To evaluate actin filament (AF)-bundle orientations quantitatively, we measured average angles and parallelness of AF-bundles by image processing. We first extracted AF-bundles as skeletonized images from confocal images by a multidirectional nonmaximum suppression (MDNMS) algorithm (Fig. S8*A*) (4). As preprocess and postprocess of MDNMS, noise in the image was reduced by a gradient inverse-weighted smoothing filter (5) and morphological filters. In the skeletonized images, angles of a neighbored pixel pair could be categorized into 0, 45, 90, and 135° against the longitudinal axis of cell, and their pixel numbers were counted, basically according to our previous study (6). The average angle is defined by

$$\theta = \begin{cases} \arctan\frac{|n_{45}-n_{135}|}{|n_0-n_{90}|+|n_{45}-n_{135}|} & \textit{if}\ n_0 \ge n_{90}\ \textit{and}\ n_{45} > n_{135} \\ 90^\circ + \arctan\frac{|n_{45}-n_{135}|}{|n_0-n_{90}|+|n_{45}-n_{135}|} & \textit{if}\ n_0 < n_{90}\ \textit{and}\ n_{45} \ge n_{135} \\ 90^\circ - \arctan\frac{|n_{45}-n_{135}|}{|n_0-n_{90}|+|n_{45}-n_{135}|} & \textit{if}\ n_0 < n_{90}\ \textit{and}\ n_{45} < n_{135} \\ 180^\circ - \arctan\frac{|n_{45}-n_{135}|}{|n_0-n_{90}|+|n_{45}-n_{135}|} & \textit{if}\ n_0 \ge n_{90}\ \textit{and}\ n_{45} < n_{135}, \end{cases} \qquad [S8]$$

where n_0, n_{45}, n_{90}, and n_{135} are the numbers of the pixel pair, which form the 0, 45, 90, and 135°, respectively. The parallelness is defined by

$$P = \frac{|n_0 - n_{90}| + |n_{45} - n_{135}|}{n_0 + n_{45} + n_{90} + n_{135}} \quad \text{[S9]}$$

and can range from 0 to 1. The parallelness becomes higher as the AF-bundles run parallel each other. All procedures were automatically performed using our ImageJ plug-ins: KbiLineExtract and KbiLineFeature, which can be invoked by Kbi_Filter2d plug-ins (filter = lineFilters, lineMode = lineExtract or lineFeature). In this study, all parameters of KbiLineExtract were fixed as follows: giwsIter = 5, mdnmsLen = 20, pickup = otsu, shaveLen = 5, delLen = 10.

RT-PCR and Genotyping. Total RNA was isolated from the 7-day-old *Arabidopsis* seedling with an RNeasy plant mini kit (Qiagen). Total RNA (1 μg) was subjected to first-strand cDNA synthesis using Ready-To-Go RT-PCR Beads (GE Healthcare). An aliquot (1 μl) was subjected to PCR with Ex Taq polymerase (Takara). The following gene-specific primers are used for RT-PCR and genotyping: MYA1-F, 5′-CTGCAATTGTTTTGCAATCCTTCCTACGAG-3′; MYA1-R, 5′-CTCGAGCCGCCTCCTGTTCCTTTACGACCA-3′; MYA2-F, 5′-AAAGATTACGTTATTGCCGAGCATCAGGCA-3′; MYA2-R2, 5′-GTGATCTTATCCATTAATTCCTGATCAACC-3′; MYA2-F3, 5′-TCGATTCTACCCTGATGAAG-3′; MYA2-R4, 5′-TCACCAAGAATGAGCAATCG-3′; XIK-F, 5′-ATCGCAAACGTATTTCCAAAGGATACAGAG-3′; XIK-R, 5′-CTCCCACAGTTGTCAAACTGAAGCTCGACA-3′; XIK-F2, 5′-GTTTCCAGAATGAAGGAAACTGAGGG-3′; XIK-R2, 5′-ACTCATATGTTAGAGGAGTAACACGG-3′; XIK-F3, 5′-CACAGGACATGACTCTTGCTGTACG-3′; XIK-R3, 5′-GCACTTTGAGGAGATCCCCTTAATCC-3′; Actin-F, 5′-AGAGATTCAGATGCCCAGAAGTCTTGTTCC-3′; Actin-R, 5′-GAGTATGATGAGGCAGGTCCAGGAATCGTT-3′; and T-DNA left border (LBa1), 5′-TGGTTCACGTAGTGGGCCATCG-3′.

Treatments with Latrunculin B and 2,3-Butanedione Monoxime. Stock solutions of reagents used were 5 mM latrunculin B (Lat B) in DMSO and 1 M 2,3-butanedione monoxime (BDM) in H_2O. Seven-day-old seedlings of GFP-h were incubated in water containing Lat B (0, 2.5, 5.0, 10, 20 μM) and BDM (0, 25, 50, 75 mM) under vacuum.

Etiolated Hypocotyls. Seeds of *Arabidopsis* were surface-sterilized and then sown onto 0.5% Gellan Gum (Wako) that contained 1% sucrose and Murasige-Skoog's medium. After incubation for 3 days at 4 °C to break seed dormancy, the plants were grown at 22 °C in the light for 2 h and then in the dark for 72 h.

Phalloidin Staining. Phalloidin staining of AF-bundles with Alexa Fluor 546 phalloidin was performed as described previously (7).

1. Hebert B, Costantino S, Wiseman PW (2005) Spatiotemporal image correlation spectroscopy (STICS) theory, verification, and application to protein velocity mapping in living CHO cells. *Biophys J* 88:3601–3614.
2. Ji L, Danuser G (2005) Tracking quasi-stationary flow of weak fluorescent signals by adaptive multi-frame correlation. *J Microsc* 220:150–167.
3. Brown CM, et al. (2006) Probing the integrin-actin linkage using high-resolution protein velocity mapping. *J Cell Sci* 119:5204–5214.
4. Sun C, Vallotton P (2009) Fast linear feature detection using multiple directional non-maximum suppression. *J Microsc* 234:147–157.
5. Wang DCC, Vagnucci AH, Li CC (1981) Gradient inverse weighted smoothing scheme and the evaluation of its performance. *Comp Graph Image Proc* 15: 167–181.
6. Yoneda A, et al. (2007) Chemical genetic screening identifies a novel inhibitor of parallel alignment of cortical microtubules and cellulose microfibrils. *Plant Cell Physiol* 48:1393–1403.
7. Tamura K, Shimada T, Kondo M, Nishimura M, Hara-Nishimura I (2005) KATAMARI1/MURUS3 Is a novel golgi membrane protein that is required for endomembrane organization in Arabidopsis. *Plant Cell* 17:1764–1776.

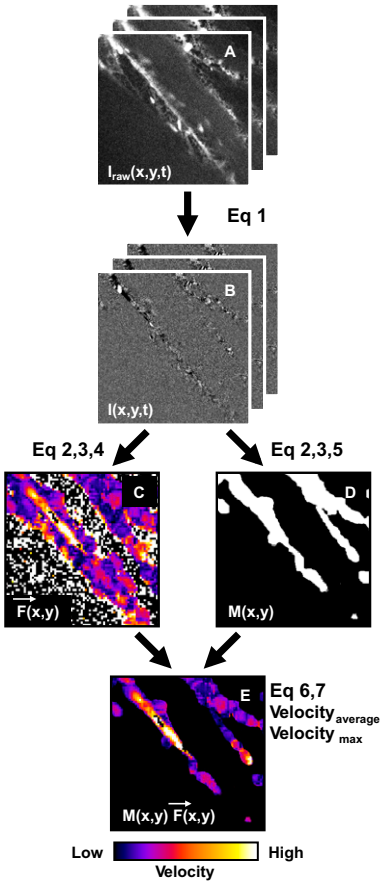

Fig. S1. Velocity-analysis scheme for endoplasmic reticulum (ER) streaming. (*A*) Original stack of time-lapse images. (*B*) Preprocessed stack. (*C*) Velocity distribution map. Color represents the velocity. Note that there are some error vectors outside of the ER regions (white pixels). (*D*) Mask image indicates ER region; white: 1, black: 0. (*E*) Masked velocity distribution map. Average and maximal velocities were calculated from *E* based on Eqs. S6 and S7.

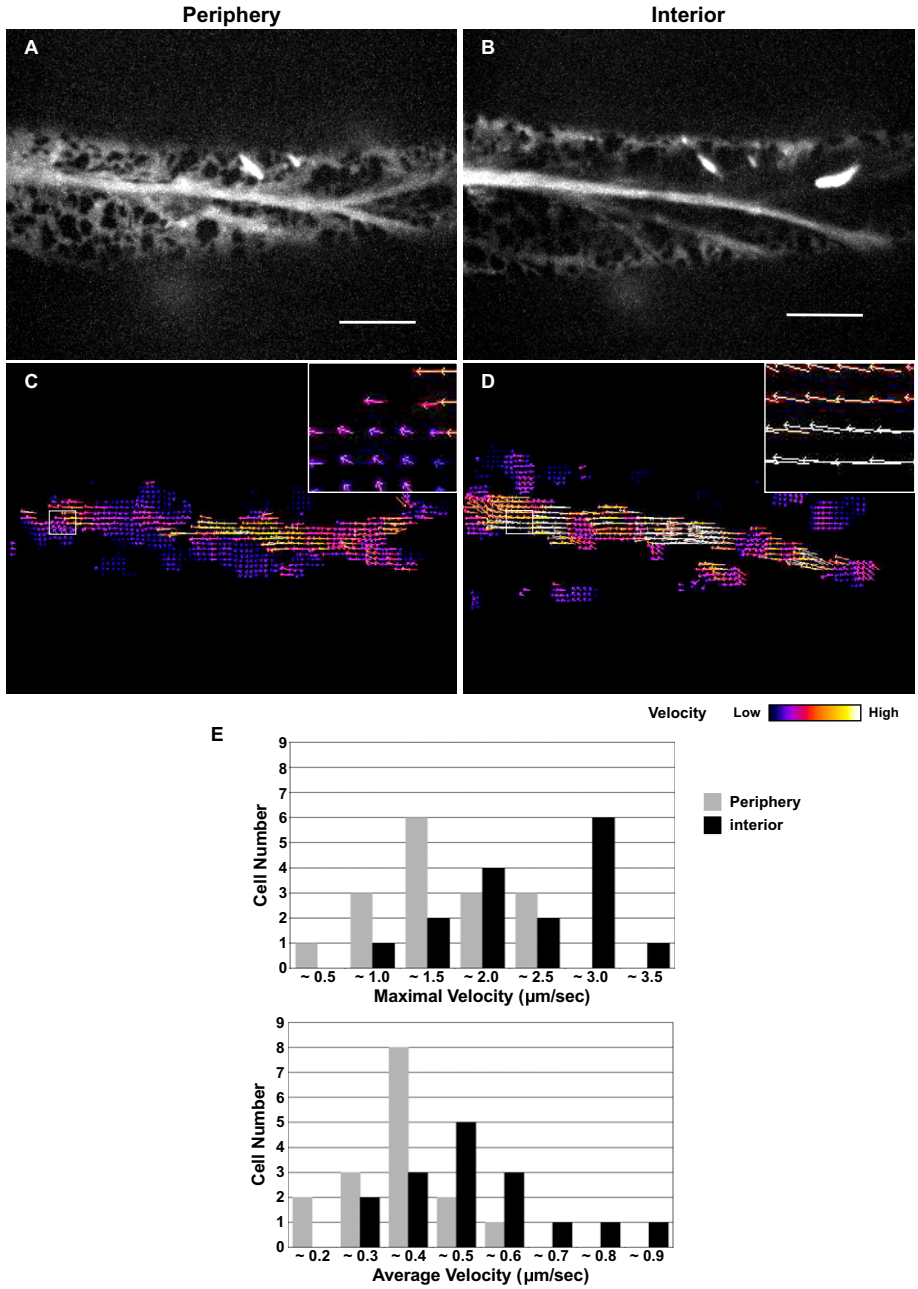

Fig. S2. ER streaming-velocity map using our developed KbiFlow software. Seven-day-old GFP-h cotyledonary petioles were observed by spinning-disk confocal microscopy. We captured 100 images of GFP-labeled ER at ~50-ms intervals in two ~1-μm thick optical planes at ~1.5 μm distance, a peripheral plane and an interior plane, of a cell. (*A* and *B*) Maximum-intensity projection of the time-lapse images of each plane. Bright trails indicate ER streaming. (Scale bars, 10 μm.) (*C* and *D*) Velocity map generated by processing the time-lapse images (*A* and *B*) with KbiFlow. Arrow lengths and colors indicate ER streaming velocities. Insets are magnified views of the boxed areas in the maps. (*E*) Histograms of the maximal velocity and the average velocity.

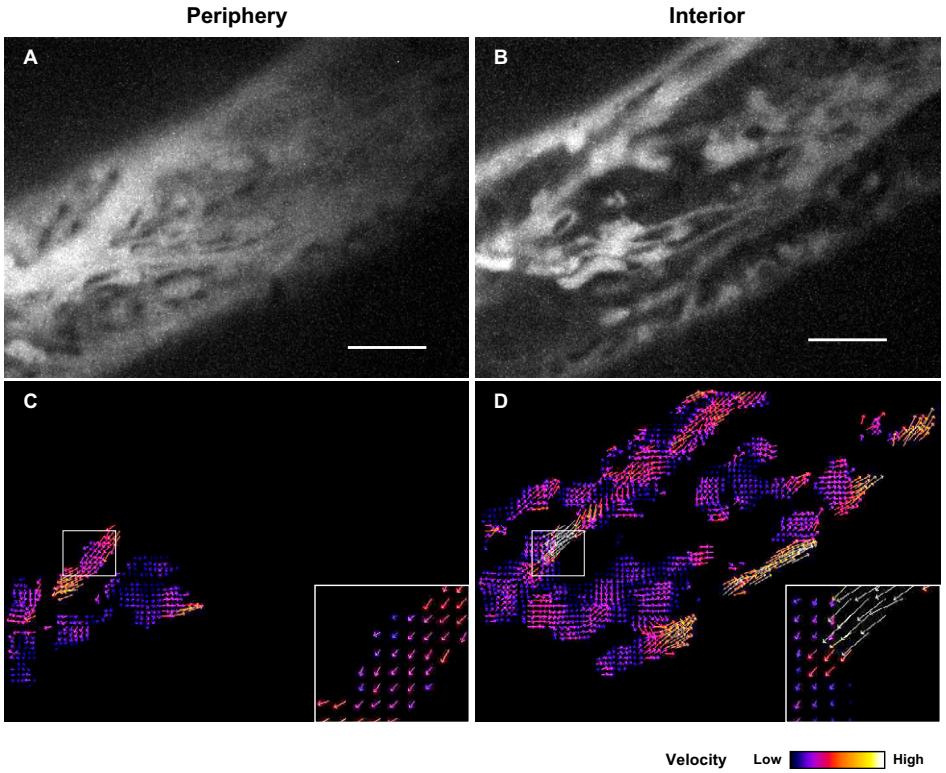

Fig. S3. Cytosol streaming velocity map using KbiFlow software. Seven-day-old cotyledonary petioles of cytosolic GFP-expressing transgenic plant were observed by spinning-disk confocal microscopy. We captured 100 images of GFP-labeled cytosol at ~50-ms intervals in two ~1-μm thick optical planes at ~1.5 μm distance, a peripheral plane and an interior plane, of a cell. (*A* and *B*) Maximum-intensity projection of the time-lapse images of each plane. Bright trails indicate cytosol streaming. (Scale bars, 10 μm.) (*C* and *D*) Velocity map generated by processing the time-lapse images (*A* and *B*) with KbiFlow. Arrow lengths and colors indicate streaming velocities. Insets are magnified views of the boxed areas in the maps.

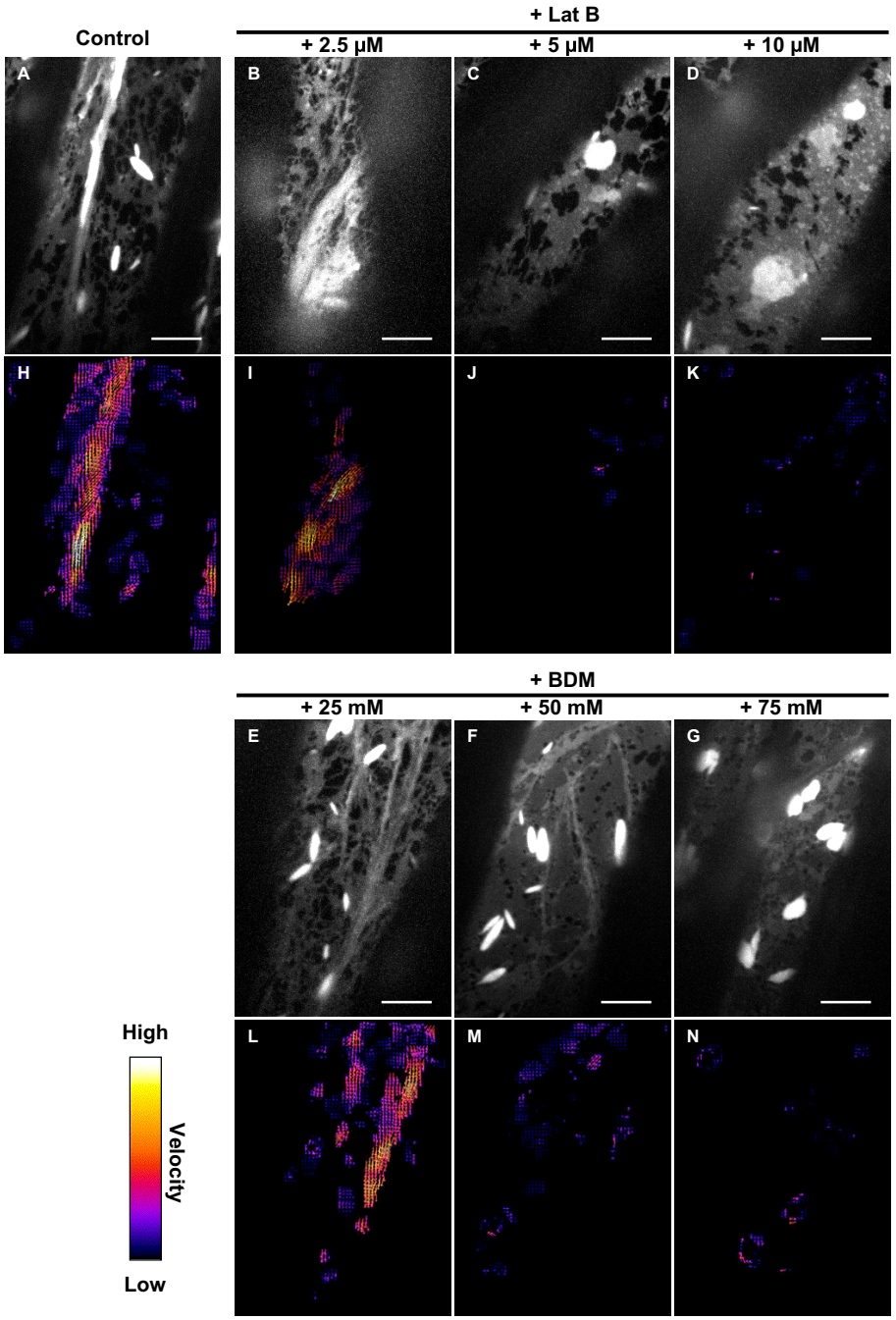

Fig. S4. ER streaming is suppressed by an inhibitor of actin polymerization or myosin inhibitor. Seven-day-old cotyledonary petioles of GFP-h were observed by spinning-disk confocal microscopy. We captured 100 images of GFP-labeled ER at ~50-ms intervals. (*A*–*G*) Maximum intensity projections of the time-lapse ER streaming images. Bright spindle-shaped structures are ER bodies. (Scale bars, 10 μm.) (*H*–*N*) Velocity maps corresponding to *A* to *G*, respectively. Velocities are represented by arrow lengths and arrow colors. (*A* and *H*) Control image. (*B*–*D* and *I*–*K*) Time-lapse images of subperipheral ER acquired after treatment with Latrunculin B (Lat B; an inhibitor of actin polymerization) for 20 min to 1.5 h. ER aggregates were forming, but they were slowly streaming after the treatment of 2.5 μM Lat B for 1.5 h. On the other hand, ER streaming was completely inhibited by the treatments with 5 or 10 μM Lat B for 40 or 20 min, respectively. (*E*–*G* and *L*–*N*) Time-lapse images of subperipheral ER acquired after treatment with 2,3-butanedione monoxime (BDM; a myosin inhibitor) for 30 min to 1 h. ER streaming was observed after the treatment of 25 mM BDM for 1 h, whereas ER streaming was completely inhibited after the treatments of 50 or 75 mM BDM for 40 min. The spindle-shaped ER bodies were collapsed by the treatment of 75 mM BDM.

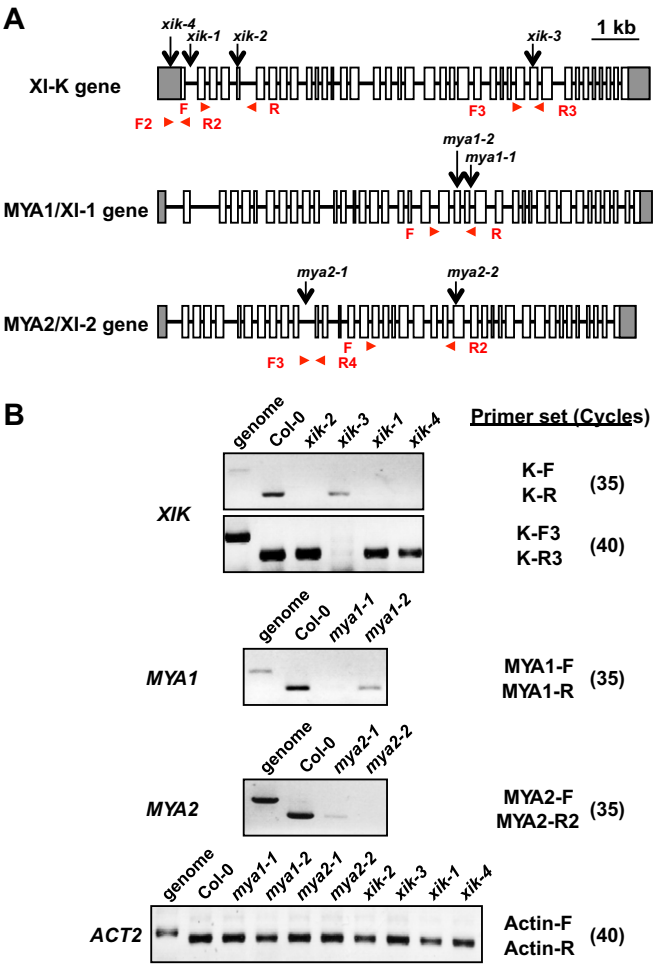

Fig. S5. Isolated myosin XI mutants. (*A*) Structures of the MYA1/XI-1, MYA2/XI-2, and XI-K genes. White boxes, gray boxes, and black lines show exons, untranslated regions, and introns, respectively. The position of each T-DNA insertion is indicated for XI-K gene (xi*k-1*, SALK_136682; xi*k-2*, SALK_067972; xi*k-3*, SALK_018764; *xik-4*, SALK_152496), MYA1/XI-1 gene (*mya1-1*, SALK_129098; *mya1-2*, SALK_022140), and MYA2/XI-2 gene (*mya2-1*, SALK_127984; *mya2-2*, SALK_055785). Primer positions for genotyping and RT-PCR are indicated by red arrowheads. (*B*) RT-PCR analysis of 7-day-old myosin mutant seedlings. The primer sets and number of amplifying cycles used are indicated to the right side of each panel. *ACT2* was used as a loading control.

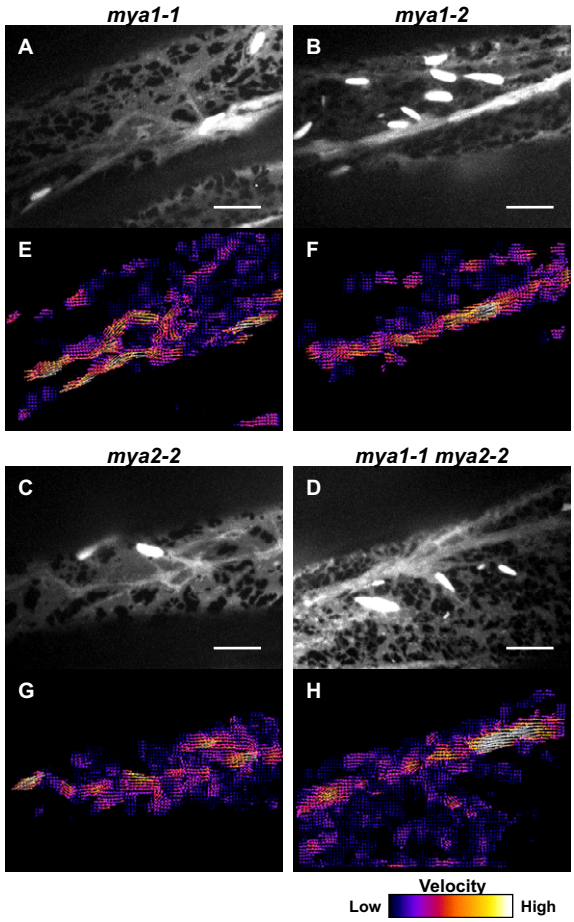

Fig. S6. ER streaming is not suppressed in MYA1/XI-1- or MYA2/XI-2-deficient mutants. Seven-day-old cotyledonary petioles of MYA1/XI-1- or MYA2/XI-2-deficient mutants expressing ER-localized GFP were observed by spinning-disk confocal microscopy. (*A–D*) Maximum intensity projections of 100 time-lapse images of the subperipheral ER captured at ~50-ms intervals. Bright spindle-shaped structures are ER bodies. (Scale bars, 10 μm.) (*E–H*) Velocity maps corresponding to *A* to *D*, respectively. ER streaming velocities are represented by arrow lengths and arrow colors.

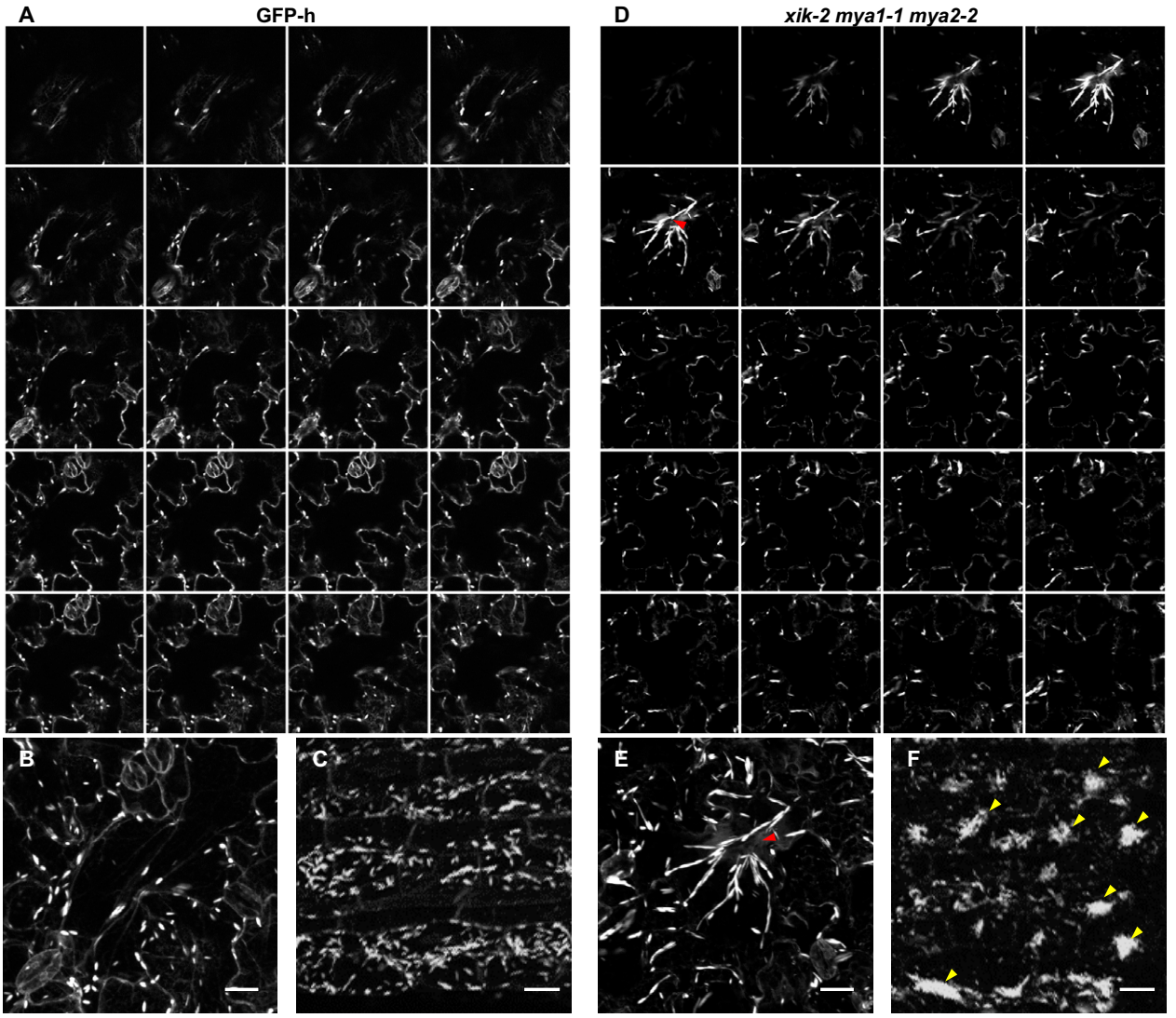

Fig. S7. Myosin XI-K deficiency induces aberrant ER body distributions. Seven-day-old seedlings of GFP-h (*A*–*C*) and *xik-2 mya1-1 mya2-2* (*D*–*F*) expressing ER-localized GFP were observed by laser-scanning confocal microscopy. (*A*, *B*, *D*, and *E*) Epidermal cotyledon cells of GFP-h (*A* and *B*) and *xik-2 mya1-1 mya2-2* (*D* and *E*). ER-body distribution patterns are shown as sequential confocal images taken along the optical *z* axis (1-μm intervals) (*A* and *D*) and their maximum intensity projections (*B* and *E*). Red arrowhead (*D* and *E*) indicates the nuclear position in a central cell. (*C* and *F*) Hypocotyls of GFP-h (*C*) and *xik-2 mya1-1 mya2-2* (*F*). ER-body distribution patterns are shown as maximum-intensity projections reconstituted from 22-sequential confocal images taken along the optical *z* axis (2-μm intervals). Yellow arrowheads (*F*) indicate aggregates of ER bodies. (Scale bars, 20 μm.)

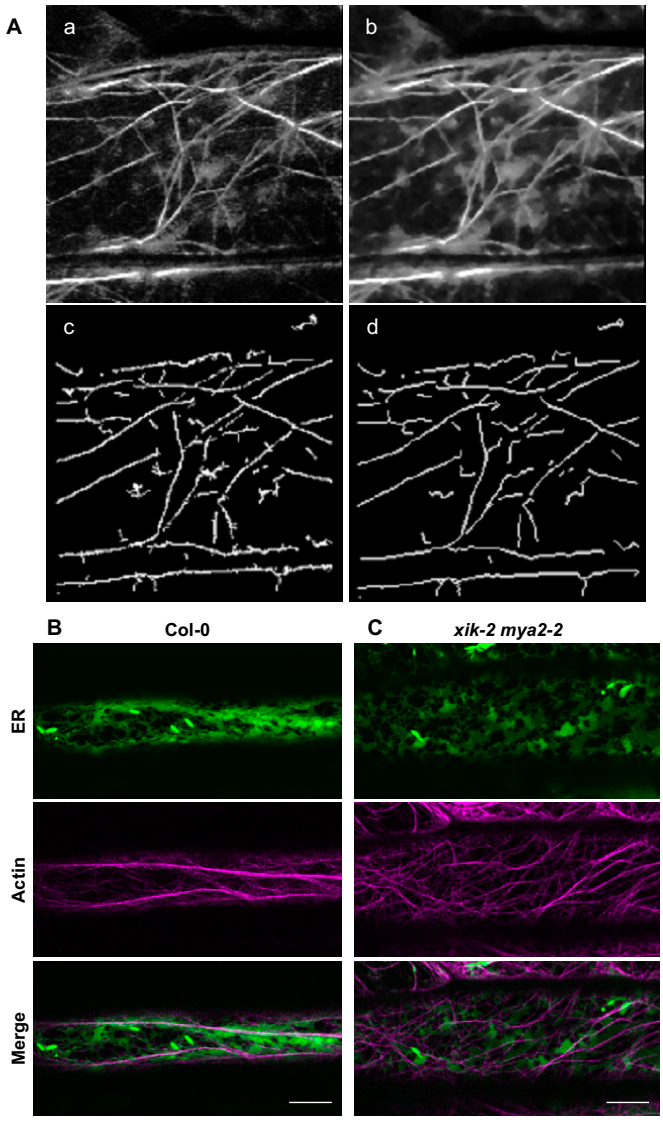

D

	Col-0	*xik-2 mya2-2*
Average angle against longitudinal axis (°)	2.49 (1.65)	6.92 (5.54)*
Parallelness	0.57 (0.07)	0.39 (0.12)**

Fig. S8. Quantitative analysis of the AF-bundle organization. (*A*) Extraction of AF bundles as skeletonized image. (*a*) An original confocal image of actin filaments visualized by tdTomato-ABD2. (*b*) Noise reduced image by gradient inverse weighted smoothing filter. (*c*) Binary image obtained from multi-directional nonmaximum suppression algorithm. (*d*) Skeletonization and noise-reduction for the binary image were performed. Average angles and parallelness were measured from the skeletonized image. (*B–D*) Myosin XI-K deficiency induces AF-bundle disorganization in the etiolated hypocotyls. Four-day-old etiolated hypocotyls of Col-0 (*B*) and *xik-2 mya2-2* (*C*) expressing ER-localized GFP and tdTomato-ABD2 were observed by laser-scanning confocal microscopy. (Scale bars, 10 μm.) Orientation of AF-bundles was evaluated by two indices: Average angle of AF-bundles against a longitudinal axis and parallelness (*D*). The value in parenthesis represents SD. *, $P < 0.005$; **, $P < 0.001$ by Student's *t* test ($n = 20–24$).

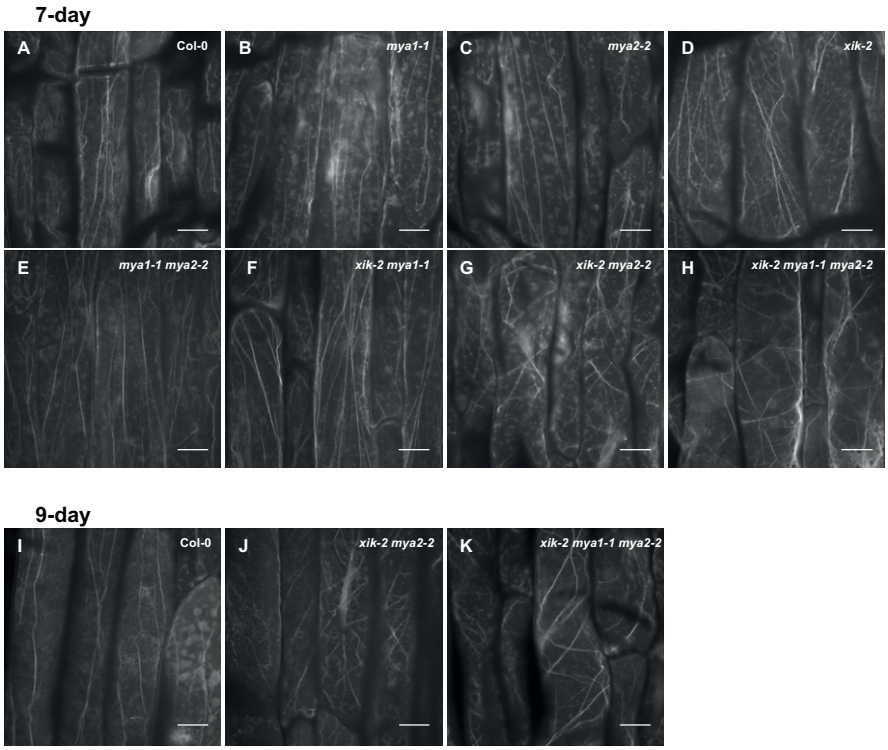

Fig. S9. Myosin XI-K deficiency induces actin filament bundle disorganization. Actin filaments in 7-day-old Col-0 (*A*), *mya1-1* (*B*), *mya2-2* (*C*), *xik-2* (*D*), *mya1-1 mya2-2* (*E*), *xik-2 mya1-1* (*F*), *xik-2 mya2-2* (*G*), and *xik-2 mya1-1 mya2-2* (*H*), and 9-day-old Col-0 (*I*), *xik-2 mya2-2* (*J*), and *xik-2 mya1-1 mya2-2* (*K*) cotyledonary petioles were stained with Alexa Fluor 546 phalloidin. Samples were observed by laser-scanning confocal microscope. (Scale bars, 20 μm.)

Table S1. Streaming velocity (μm/sec) of ER and cytosolic GFP measured by KbiFlow software

Plant	Number of cells	Maximal velocities	SD	SE	Average velocities	SD	SE
GFP-h							
Interior	16	2.196	0.709	0.177	0.482	0.173	0.043
Periphery	16	1.353	0.622	0.156	0.329	0.110	0.028
Cytosolic GFP							
Interior	22	1.989	0.755	0.161	0.493	0.199	0.043
Periphery	22	1.225	0.424	0.090	0.365	0.115	0.024
GFP-h	42	2.062	0.653	0.119	0.417	0.122	0.022
xik-1	29	0.757	0.345	0.064	0.219	0.099	0.018
xik-2	57	0.682	0.297	0.039	0.204	0.076	0.010
mya1-1	30	2.041	0.959	0.175	0.379	0.150	0.027
mya1-2	36	1.888	0.816	0.149	0.412	0.240	0.044
mya2-2	30	1.812	0.621	0.113	0.392	0.131	0.024
xik-2 mya1-1	30	0.503	0.259	0.047	0.143	0.050	0.009
xik-2 mya2-2	28	0.646	0.291	0.055	0.178	0.052	0.010
mya1-1 mya2-2	30	1.816	0.610	0.111	0.350	0.104	0.019
xik-2 mya1-1 mya2-2	34	0.394	0.196	0.034	0.118	0.030	0.005
xik-1 mya1-2 mya2-1	35	0.332	0.162	0.028	0.121	0.036	0.006

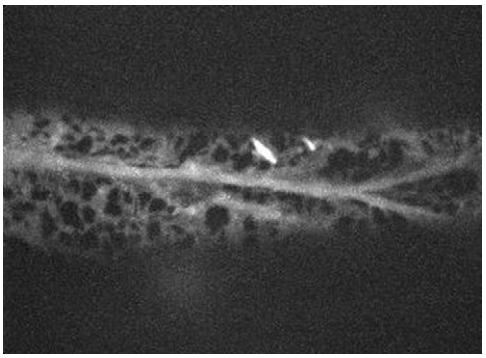

Movie S1. ER streaming in GFP-h. This is a real-time movie corresponding to Fig. S2*A*.

Movie S1

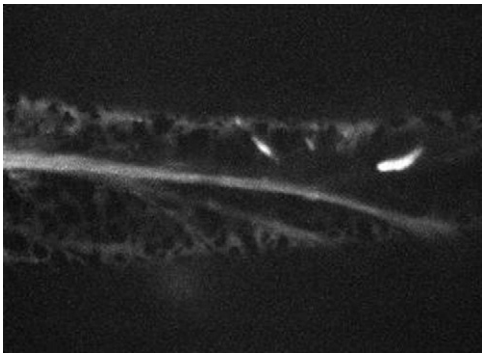

Movie S2. ER streaming in GFP-h. This is a real-time movie corresponding to Fig. S2*B*.

Movie S2

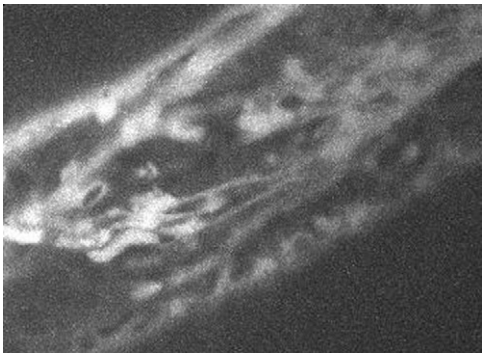

Movie S3. Streaming of cytosolic GFP. This is a real-time movie corresponding to Fig. S3*B*.

Movie S3

Movie S4. ER streaming is suppressed with an inhibitor of actin polymerization. This is a real-time movie corresponding to Fig. S4*C*.

Movie S4

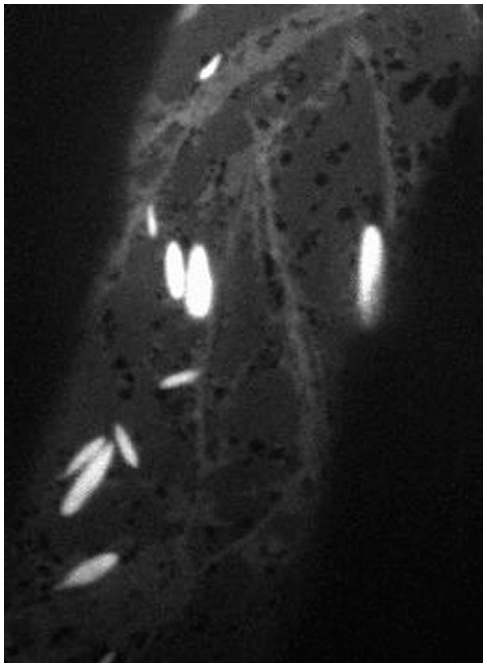

Movie S5. ER streaming is suppressed with a myosin inhibitor. This is a real-time movie corresponding to Fig. S4*F*.

Movie S5

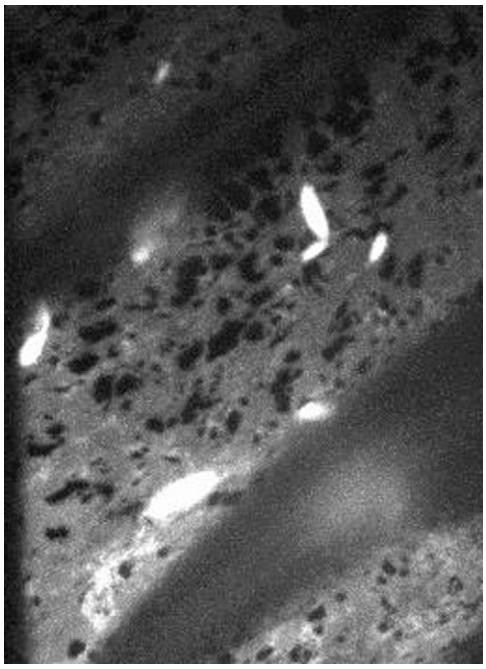

Movie S6. ER streaming is suppressed in *xik*. This is a real-time movie corresponding to Fig. 1*B*.

Movie S6

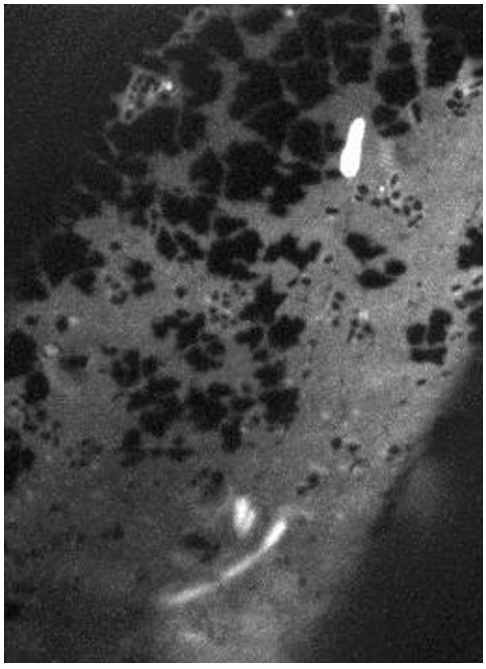

Movie S7. ER streaming is suppressed in *xik mya1 mya2*. This is a real-time movie corresponding to Fig. 1*F*.

Movie S7

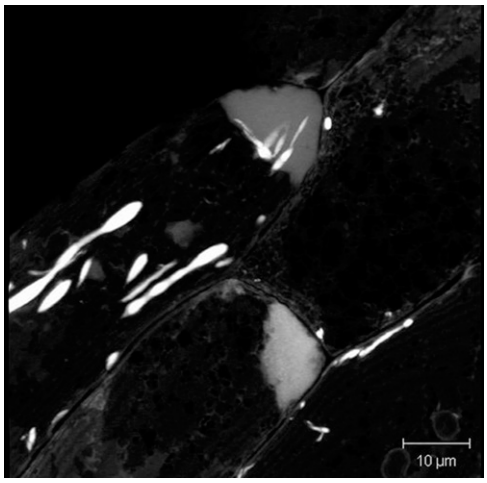

Movie S8. ER aggregates in *xik mya1 mya2*. ER aggregates corresponding to Fig. 3*G* are shown as 3D structures that were reconstituted from 14 sequential, confocal images taken along the optical *z* axis (1-μm intervals).

Movie S8

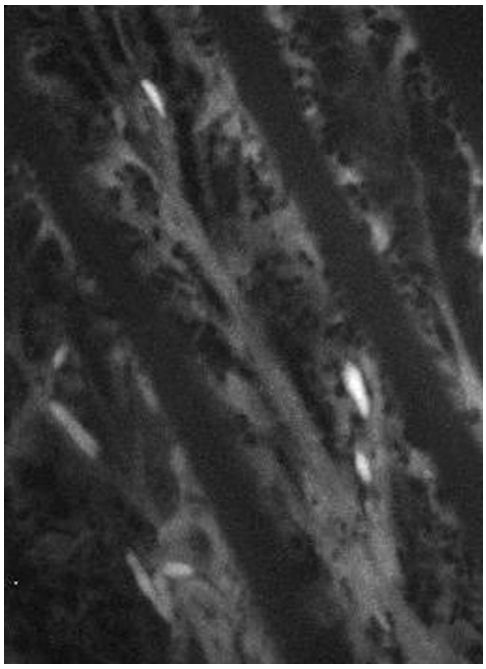

Movie S9. ER streaming in the elongating cell of etiolated GFP-h hypocotyl. This is a real-time movie.

Movie S9

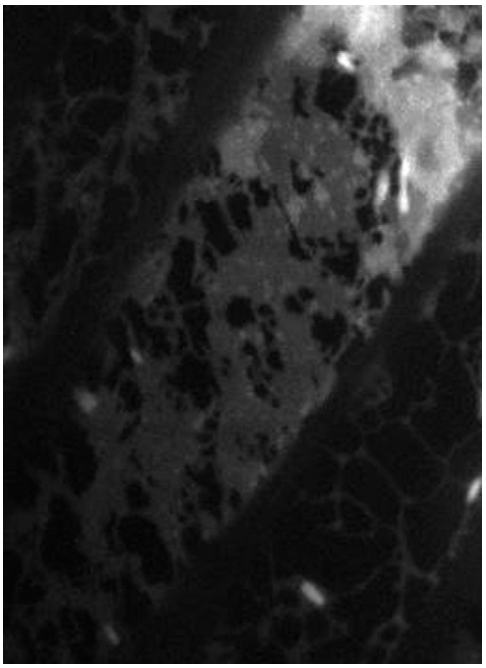

Movie S10. ER streaming is suppressed in the elongating cell of etiolated *xik mya2* hypocotyl. This is a real-time movie.

Movie S10